Frequency-dependent Scattering of Wideband Laser-generated Rayleigh Waves for Vertical Surface Crack Characterization

Lei Xu[a,1,*], Yiyin Su[b,1], Jianwei Yang[a] and Zhongqing Su[c]

[a] Robotics and Artificial Intelligence Division, Hong Kong Productivity Council, Kowloon, Hong Kong SAR

[b] Research Center for Humanoid Sensing, Zhejiang Lab, Kechuang Avenue, Hangzhou, Zhejiang Province, China

[c] Department of Mechanical Engineering
The Hong Kong Polytechnic University, Kowloon, Hong Kong SAR

submitted to ***Smart Materials and Structures***

(Submitted on 8th December 2022, revised and re-submitted on 14th January 2023)

[*] To whom correspondence should be addressed. Tel.: +852-5939-8557.
[1] Lei Xu and Yiyin Su contributed equally to this work.
Email: leixu@hkpc.org (Lei Xu, *Ph.D*)

Abstract

Wideband laser-generated Rayleigh waves have been extensively exploited for surface crack characterization, most of which, nonetheless, are of a nature of either numerical simulation or experimental observation. Earlier, an elastodynamic reciprocity theorem-based theoretical model was proposed by the authors [1, 2], aimed at scrutinizing the interaction of narrowband Rayleigh-Lamb waves with a surface or subsurface crack. In this study, the model is expanded to a wideband scenario to analytically explore the interaction of a wideband laser-generated Rayleigh wave with a surface crack, as well as the resultant crack-scattered Rayleigh wavefield. First, under the narrowband scenario, a dimensionless parameter is formulated based on the closed-form solution to the magnitude of the narrowband scattered Rayleigh wavefield, revealing that the scattering effect of a surface crack on the Rayleigh waves is frequency-dependent and there exists a characteristic frequency, at which the crack-scattered Rayleigh wavefield manifests the strongest intensity. Similarly, under the wideband scenario, such dependence can be calibrated by a spectral damage indicator (SDI), which facilitates the evaluation of the severity of the surface crack using the wideband laser-generated Rayleigh wave. Proof-of-concept simulation is performed to verify the model. Quantitative agreement between the analytical and numerical results validates the accuracy of the proposed model and SDI. Experiment is also conducted to demonstrate the effectiveness of the frequency-dependent scattering of wideband laser-generated Rayleigh waves for vertical surface crack characterization.

***Keywords*:** Laser-generated Rayleigh wave; frequency-dependent scattering; spectral damage indicator; vertical surface crack; experimental validation

1. Introduction

Surface crack is one of the typical types of defects in metallic structures which can grow subjected to cyclic loading, remarkably jeopardizing structural integrity and posing as a major cause of failures in different mechanical structures. Therefore, it is of great significance to identify and evaluate surface cracks before they develop to critical sizes. A number of nondestructive evaluation techniques have been developed for the detection and characterization of surface cracks, which broadly embrace those making use of bulk waves [3, 4], Rayleigh-Lamb waves [5-13], and acoustic emission [14] to name a few. With the wave energy dominance near to the waveguide surface, Rayleigh waves have been employed to identify structural damage near structural surface. Representatively, the amplitude of Rayleigh wave was utilized to characterize the depth of surface crack in concrete [15-17] and metallic materials [18], respectively. Ahmad *et. al.* [19] used the reflection and transmission coefficients of Rayleigh waves generated by electromagnetic acoustic transducers (EMATs) to quantify the width of surface cracks. For identifying small-scale structural damage, nonlinear Rayleigh wave [20-22] is gaining more and more attention due to its superior sensitivity to microscopic damage. These techniques have to be applied by virtue of contact-type transducers that are mounted or placed on the sample surface, which greatly restricts the practical implementation of these techniques in some severe testing environments (*i.e.*, irregular surface, high temperature and pressure).

Recently, the laser ultrasonic technique (LUT) has been widely exploited for the detection and evaluation of various types of structural damage [23-28], due to its superior merits such as the noncontact excitation and wideband reception of ultrasonic waves, high sensitivity to damage and spatial resolution, accessibility to harsh environments and complexed structures. According to numerical and experimental results, multiple types of ultrasonic waves can be generated by a pulsed laser beam, including the skimming longitudinal wave, body longitudinal wave, shear wave, and Rayleigh wave. Amongst these laser-generated ultrasonic waves, the Rayleigh wave

has the remarkably stronger magnitude compared with the other waves, resulting in extensive utilization of the laser-generated Rayleigh wave in LUT-based damage detection schemes. Dixon *et. al.* [29] found that the arrival time of crack-scattered laser-generated Rayleigh wave is related to crack depth, which can be used for quantitative evaluation of surface cracks. To identify fatigue cracks in aluminum and steel plates, Sohn *et. al.* [30] proposed a dual laser excitation technique to generate wideband and narrowband ultrasonic waves simultaneously, by adjusting the laser beam sizes of two pulsed excitation lasers. By counting the sideband peaks of acquired signals, fatigue cracks smaller than 0.1 mm can be detected. Zhou *et. al.* [31] investigated the interaction of laser-generated Rayleigh wave with a surface crack and adopted the reflection and transmission coefficients for crack depth gauging. It was found that the wave reflection is non-monotonically related to the frequency of probing Rayleigh waves and the transmission shows approximately linear decrease with respect to crack depth, which can be used for quantitative characterization of surface cracks. Chen *et.al.* [32] reported a phase evolution phenomenon of laser-generated Rayleigh wave upon interacting with a subsurface defect, which was observed in both numerical simulation and experiments. A dimensionless parameter, defined as the ratio of absolute negative peak to positive peak of Rayleigh wave, was proposed to evaluate subsurface defects. Zeng *et. al.* [33-36] performed systematic finite element (FE) simulation to examine the interaction of laser-generated ultrasonic waves with different types of damage in both plates and cylinder pipes, including surface/subsurface cracks, angled cracks and branched-breaking defects.

With that being said, most of the previous research exploring the interaction of a laser-generated Rayleigh wave with a surface crack for crack identification and characterization, are of a nature of either numerical simulation or experimental investigation, and there is obvious lack of theoretical interrogation to shed light on the interaction of a laser-generated Rayleigh wave with a surface crack, as well as the resultant crack-scattered Rayleigh wavefield. Earlier, the authors of this paper proposed a theoretical model based on elastodynamic reciprocity theorem, to interpret

98 the interaction of narrowband Rayleigh-Lamb waves with non-penetrating fatigue cracks and
99 surface/subsurface cracks [1, 2, 37]. Closed-form solutions to the magnitude of crack-scattered
100 waves were derived, based on which the severity of a crack can be evaluated quantitatively. The
101 accuracy of the model and closed-form solution has been validated by both numerical simulation
102 and experiments. Nevertheless, the model cannot be straightforward applied to explore the
103 interaction of the laser-generated Rayleigh wave with a crack, owing to the laser-generated
104 Rayleigh wave has a feature of wide frequency band and the scattering of Rayleigh wave of
105 different frequencies by a crack is not identical [31].
106
107 Motivated by this, the elastodynamic reciprocity theorem-based model is expanded to the
108 wideband scenario, to investigate the scattering of the laser-generated Rayleigh wave by a surface
109 crack. To this end, the narrowband Rayleigh waves of different frequencies scattered by a surface
110 crack is first investigated, to obtain the dependence of wave scattering on the central frequency of
111 the incident Rayleigh wave. The characteristic frequency, at which the scattered Rayleigh
112 wavefield manifests the strongest intensity, is analytically derived. For the laser-generated
113 Rayleigh wave which has a wide frequency band, wave components in different frequency ranges
114 are distinctively scattered by the surface crack. To make use of the frequency-dependent scattering
115 of Rayleigh wave for surface crack characterization, a spectral damage indicator (SDI), defined
116 as the ratio of the spectral density of the crack-scattered Rayleigh wave to that of the incident
117 Rayleigh wave, is proposed. By virtue of the SDI, the characteristic frequency can be determined,
118 via which the severity of a surface crack can be quantitatively evaluated. Proof-of-concept FE
119 simulation is conducted to explore the interaction of wideband laser-generated Rayleigh wave
120 with a vertical surface crack. Experiment is subsequently performed to demonstrate the
121 effectiveness of the frequency-dependent scattering of the wideband laser-generated Rayleigh
122 wave for vertical surface crack characterization.
123

2. Scattering of Rayleigh Wavefield by a Surface Crack: A Theoretical Perspective

To analytically scrutinize the interaction of a wideband laser-generated Rayleigh wave with a surface crack and the resultant crack-scattered wavefield, the elastodynamic reciprocity theorem-based analytical model previously developed for investigating the scattering of narrowband Rayleigh wave by a surface crack, is recapitulated in Section 2.1. Subsequently, the model is extended to the wideband scenario to explore the scattering of a laser-generated Rayleigh wave by a surface crack, in Section 2.2.

2.1 Elastodynamic Depiction of Crack-scattered Rayleigh Wavefield

Elastodynamic reciprocity theorem has been widely adopted by a number of researchers to examine the scattering of ultrasonic waves by defects [38-41]. By jointly utilizing this theorem and a virtual wave method, the authors proposed a theoretical model to study the nonlinear interaction of a narrowband Rayleigh wave with a surface crack featuring opening-closing behavior during wave propagation and obtained a closed-form solution to the magnitude of crack-scattered second harmonic of Rayleigh wave. In a 2D, half-space defined by $x-z$ coordinates, the displacements of a time-harmonic Rayleigh wave in an isotropic, homogenous, and linearly elastic waveguide can be defined, along the positive x direction, as

$$u_x^{incident}(x,z) = \pm iA_{in}U^R(z)e^{\pm ikx}, \tag{1}$$

$$u_z^{incident}(x,z) = A_{in}W^R(z)e^{\pm ikx}. \tag{2}$$

In the above, A_{in} signifies the magnitude of the incident Rayleigh wave and i the imaginary unit, and k is the wavenumber ($k=\omega/C_R$, where ω and C_R denotes the circular frequency and the velocity of the Rayleigh wave, respectively). $u_x^{incident}(x,z)$ and $u_z^{incident}(x,z)$ represent the particulate displacement components of the Rayleigh wave in the x direction and z direction, respectively. The plus and minus signs in Eq. (1) indicate wave propagation in the positive and

148 negative x direction, respectively. Functions $U^R(z)$ and $W^R(z)$ are related to the mechanical
149 properties of the waveguide and the frequency of the Rayleigh wave. Complete definition of the
150 two functions can be found in many textbooks [42] and papers [43] on ultrasonics.
151
152 A propagating Rayleigh wave can be scattered if there exists a surface crack in the waveguide, as
153 illustrated in **Fig.1**. If the sensing point locates between the wave excitation point and the crack,
154 the crack-scattered wave is the back-scattered wave. Otherwise, if the crack is between excitation
155 and sensing points, the crack-scattered wave should be the transmitted wave. By making use of
156 the elastodynamic reciprocity theorem, in conjunction with a virtual wave method, the magnitude
157 of the displacement of the narrowband Rayleigh wave backscattered by an open surface crack can
158 be expressed in an explicit manner, as

159 $$u_x^{scattered} = \frac{\pi(1-\nu)L^2 A_{in}\{[T_{xx}(L/2)]^2 - [T_{xz}(L/2)]^2\}}{4\mu I} U^R(z)e^{ikx}, \quad (3)$$

160 $$u_z^{scattered} = \frac{i\pi(1-\nu)L^2 A_{in}\{[T_{xx}(L/2)]^2 - [T_{xz}(L/2)]^2\}}{4\mu I} W^R(z)e^{ikx}. \quad (4)$$

161 In the above, υ is the Poisson's ratio, μ is the second Lame constant, and L is the depth of the
162 surface crack. T_{xx} and T_{xz} are functions dependent on the mechanical properties of the
163 waveguide, the frequency of the Rayleigh wave and the crack depth. I is an integral of the
164 product of stress and displacement of the Rayleigh wave along the depth direction of the
165 waveguide. Interested readers are referred to for detailed modeling process and mathematical
166 derivation of the above solution. It should be noted that in the mathematical derivation, the static
167 crack opening displacement under a uniform load at the crack surface is used to define the crack
168 opening displacement during wave propagation, which is tenable only when the crack depth is
169 smaller than the wavelength of the incident Rayleigh wave. Therefore, Eqs. (3) and (4) are
170 applicable for surface cracks with lengths smaller than the wavelength of the incident wave. Based
171 on the explicit expression of the magnitude of crack-scattered Rayleigh wave, a dimensionless

parameter β, defined as the ratio of the magnitude of crack-scattered Rayleigh wave to that of the incident Rayleigh wave, is proposed to indicate the scattering effect of a surface crack on the propagating Rayleigh wave, as

$$\beta = \frac{\pi(1-\nu)L^2\{[T_{xx}(L/2)]^2 - [T_{xz}(L/2)]^2\}}{4\mu I}. \quad (5)$$

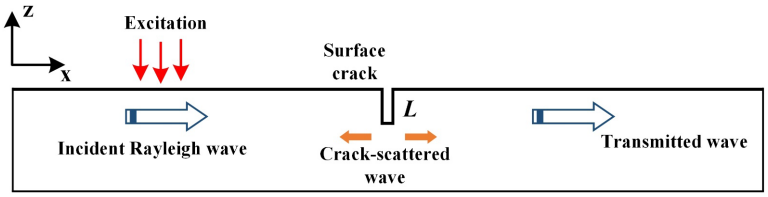

Figure 1. Illustration of a propagating Rayleigh wave scattered by a surface crack.

According to Eq. (5), the dependence of the defined dimensionless parameter β on the central frequency of the incident narrowband Rayleigh wave is illustrated in **Fig. 2(a)**, from which it can be observed that for surface cracks with different severities (crack depth varies from 0.2 mm to 0.6 mm with an interval of 0.1 mm), β increases first and then decreases, showing a parabolic relationship against the incident frequency. There exists a characteristic frequency for each surface crack, at which the crack-scattered Rayleigh wavefield manifests the largest intensity, indicating that the scattering effect of the crack on a Rayleigh wave is stronger at the characteristic frequency, compared with other frequencies.

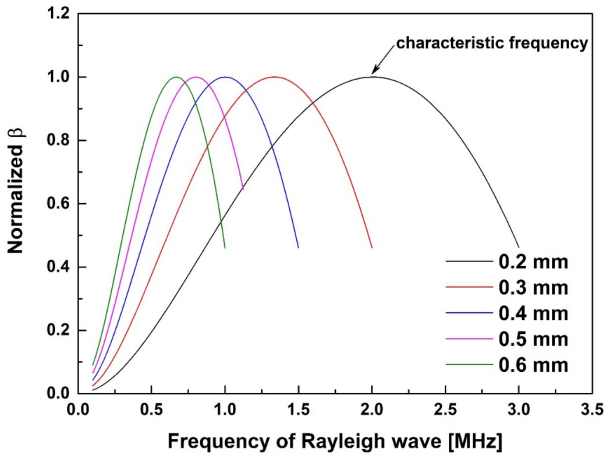

(a)

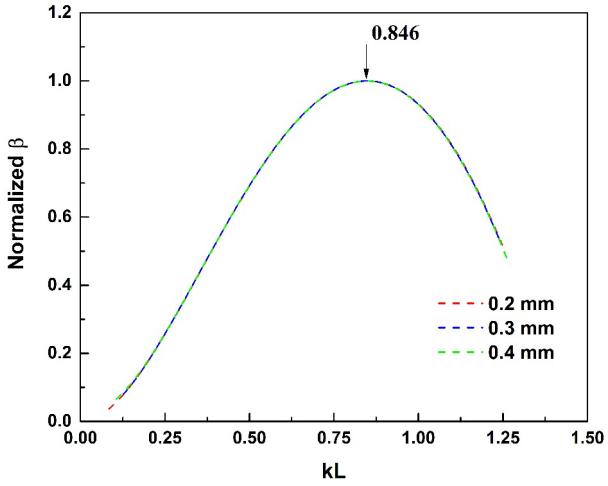

(b)

Figure 2. Normalized β with respect to (a) the central frequency of the incident Rayleigh wave, and (b) the dimensionless frequency kL for surface cracks of different depths.

If β is plotted with respect to a dimensionless frequency kL ($kL = \omega L / C_R$), as shown in **Fig. 2(b)**, it can be found that distinct curves of the relationship between β and the frequency of Rayleigh wave for surface cracks with various depths converge to a unified curve. For surface cracks with different depths, the scattering effect is the strongest when the dimensionless frequency equals to 0.846, which can be used for the calculation of the characteristic frequencies for surface cracks with different severities, as depicted in **Fig. 3**. It is noteworthy that the explicit expressions of the magnitudes of crack-scattered Rayleigh wave (Eqs. (3) and (4)) are applicable for small surface cracks with depths largely smaller than the wavelength of the incident wave, **Fig. 2** illustrates the maximum value of β in the low kL range. The accuracy of the analytical result of the characteristic frequency for surface cracks with different depths is to be verified by FE simulation in Section 3.

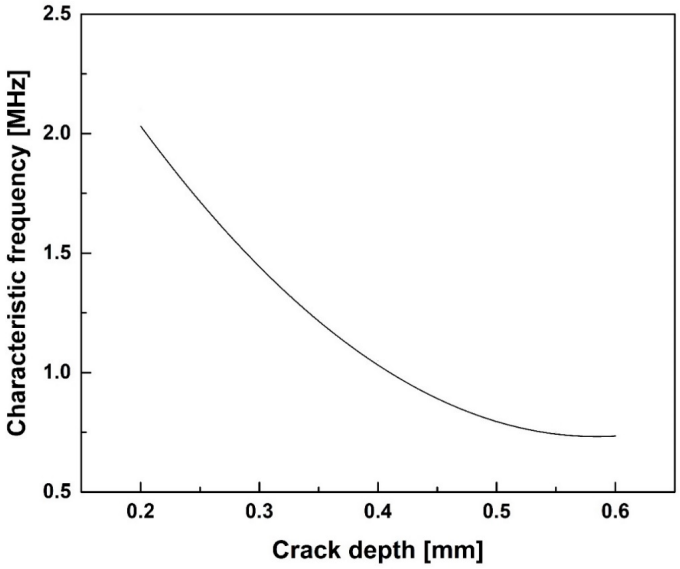

Figure 3. Analytical result of the characteristic frequency for surface cracks with various depths.

2.2 Scattering of Wideband Rayleigh Wave by A Surface Crack

If the incident Rayleigh wave has a broad frequency range (*i.e.*, the wideband laser-generated Rayleigh wave), the crack-scattered Rayleigh wave is also wideband. A representative wideband Rayleigh wave scattered by a surface crack is shown in **Fig. 4**, as well as the spectra of both the incident and crack-scattered Rayleigh waves. It can be easily observed from **Fig. 4(b)** that the central frequencies of the incident and crack-scattered Rayleigh waves are largely the same (around 1.2 MHz), and the wave energy is mainly concentrated in the range of 0-3 MHz for the two waves. Nonetheless, the distributions of the wave energy of the incident and crack-scattered Rayleigh wave are different, revealing that the scattering of the Rayleigh wave components in various frequency ranges by a surface crack is not identical, which is in accordance with the conclusion of the narrowband scenario in Section 2.1.

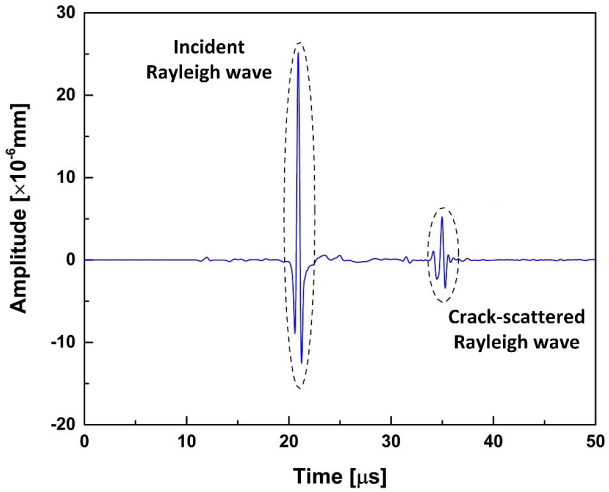

(a)

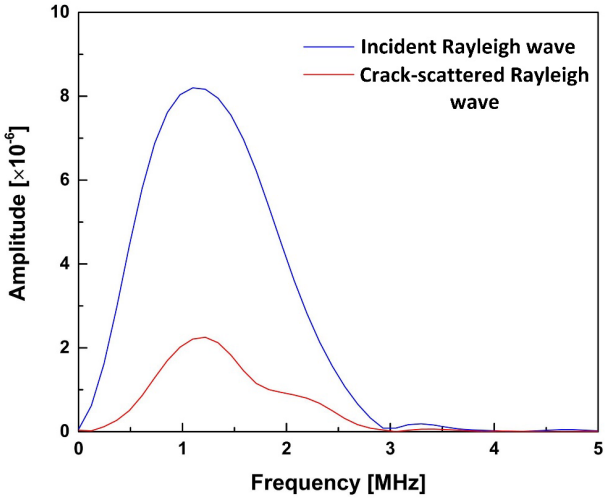

(b)

Figure 4. (a) A representative wideband Rayleigh wave scattered by a surface crack, and (b) the spectra of the incident and back-scattered Rayleigh wave.

To characterize the scattering effect of a surface crack on a wideband Rayleigh wave and make use of the frequency-dependent scattering of wideband Rayleigh wave for the evaluation of surface cracks, an SDI, $\chi(f)$, is defined based on the spectral density of the incident and the crack-scattered Rayleigh waves (*i.e.*, back-scattered wave or transmitted wave), as

$$\chi(f) = \frac{U^{scattered}(f)}{U^{incident}(f)}, \tag{6}$$

where $U^{scattered}(f)$ and $U^{incident}(f)$ are the power spectrum of fast Fourier transform (FFT) of the back-scattered/transmitted Rayleigh wave and incident Rayleigh wave ($u^{scattered}$ and $u^{incident}$),

237 respectively. Different from the parameter β which is defined as the magnitudes of the
238 narrowband time-domain incident and crack-scattered Rayleigh wave signals, the SDI is defined
239 based on the frequency-domain spectral density functions of the wideband incident and crack-
240 scattered Rayleigh waves. Such definition makes the SDI capable of revealing the different
241 scattering degrees of a wideband Rayleigh wave in distinct frequency ranges, which is different
242 from the parameter β.
243
244 According to the definition of the SDI, for the $\chi(f)$ determined by the back-scattered Rayleigh
245 wave, the higher value of $\chi(f)$ indicates that the surface crack has a stronger scattering effect on
246 the wave component at frequency f, and the SDI reaches its maximum at the characteristic
247 frequency at which the scattering effect is the strongest compared with other frequencies in the
248 broad frequency range of the incident wideband Rayleigh wave. On the contrary, for the $\chi(f)$
249 determined by the transmitted Rayleigh wave, the lower value of $\chi(f)$ indicates that the surface
250 crack has a stronger scattering effect on the wave component at frequency f, and the SDI
251 reaches its minimum at the characteristic frequency at which the scattering effect is the strongest.
252 Take the back-scattered Rayleigh wave shown in **Fig. 4** as an example, the SDI is calculated and
253 depicted in **Fig. 5**. It can be found that the SDI reaches its maximum at the characteristic frequency
254 (around 1.221 MHz), indicating that the scattering effect is stronger at this frequency than other
255 frequency ranges.
256

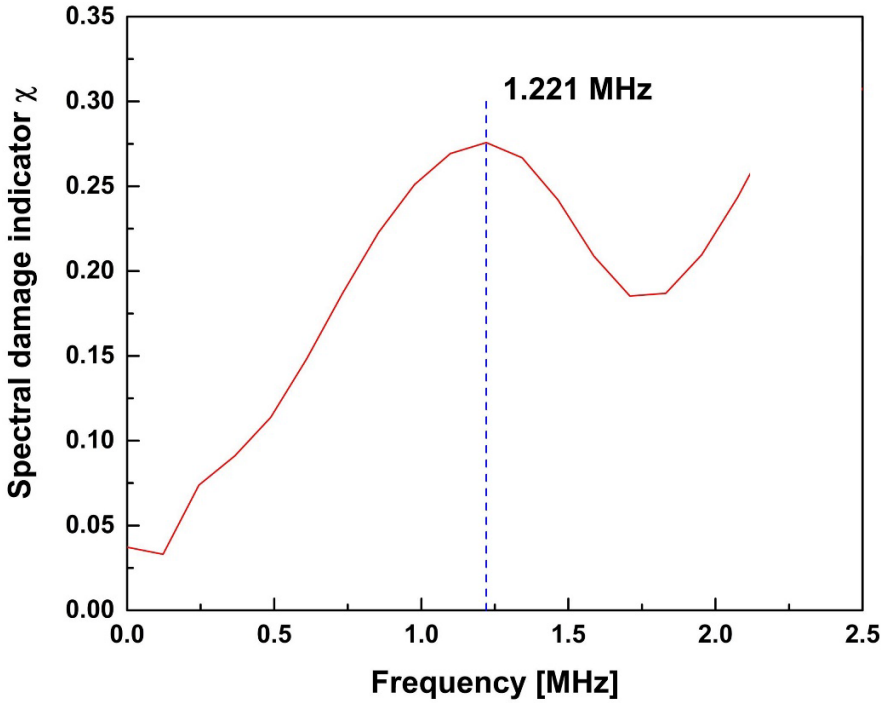

Figure 5. The SDI of the crack-scattered Rayleigh wave.

By finding the maximum value of the SDI determined by the back-scattered wave or the minimum value of the SDI determined by the transmitted wave, the characteristic frequency of the surface crack can be identified, via which the depth of the surface crack can be evaluated according to the relationship between the characteristic frequency and the depth of the surface crack. It is noteworthy that the explicit expressions of the magnitude of crack-scattered Rayleigh wave (Eqs. (3) and (4)) are applicable for a surface crack with its depth being smaller than the wavelength of the incident wave. For this sake, the defined SDI is useful for the characterization of small surface cracks. The effectiveness of the SDI for depth characterization of small surface cracks is to be verified by FE simulation in Section 3 and experiment in Section 4.

3. Proof-of-concept Numerical Simulation

Two-dimensional (2D) FE simulation is performed in this section to validate the frequency-dependent scattering of a narrowband Rayleigh wave first and verify the accuracy of the analytical result of the characteristic frequency of a small surface crack. Subsequently, multi-physical FE

simulation is conducted to simulate the interaction of the wideband laser-generated Rayleigh wave with a vertical surface crack, to demonstrate the effectiveness of the frequency-dependent scattering of laser-generated Rayleigh wave for vertical surface crack characterization.

3.1 Finite Element Model Set-up

To verify the scattering of a narrowband Rayleigh wave by a surface crack and the analytical results of the characteristic frequency, a 2D, plate-like aluminum waveguide (Young's modulus: 73 GPa; Poisson's ratio: 0.33; density: 2700 kg/m^3) with a surface crack is considered, as shown in **Fig. 6**. The thickness of the waveguide is 20 mm, to ensure that the Rayleigh wave can be generated. A sensing point is set between the excitation point and the surface crack, to acquire the incident and back-scattered Rayleigh waves. To guarantee the simulation accuracy, the integral time is 0.2 ns and a fine FE mesh is applied in which the maximum mesh size is 0.1 mm – that is about 1/15 of the minimal wavelength of the incident Rayleigh waves.

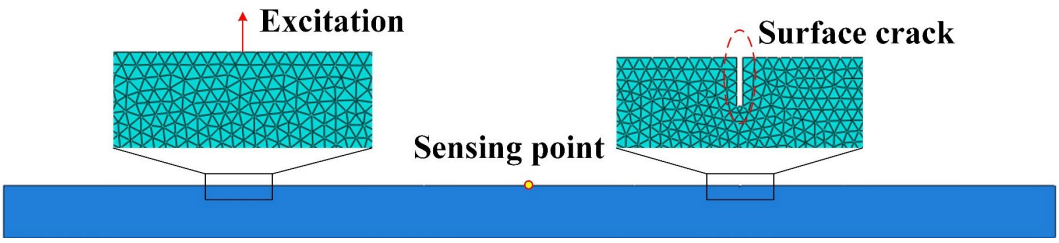

Figure. 6 FE model for validation of narrowband Rayleigh wave scattering by a surface crack.

5-cycle Hanning-windowed sinusoidal tonebursts at different central frequencies are excited by applying a displacement for a point on the top surface of the waveguide, to generate narrowband Rayleigh waves. A typical narrowband excitation signal with a central frequency of 1 MHz and its spectrum are illustrated in **Fig. 7(a-b)**, respectively. The propagating Rayleigh wave scattered by a surface crack is captured by the sensing point on the surface of the waveguide, as shown in **Fig. 7(c)**. By comparing the magnitudes of the crack-scattered and the incident Rayleigh waves, the dimensionless parameter β can be determined, which can be used to reveal the different

scattering effect of the surface crack on incident narrowband Rayleigh wave with various central frequencies. In the simulation, the depth of the vertical surface crack varies from 0.2 mm to 0.6 mm, with an interval of 0.1 mm.

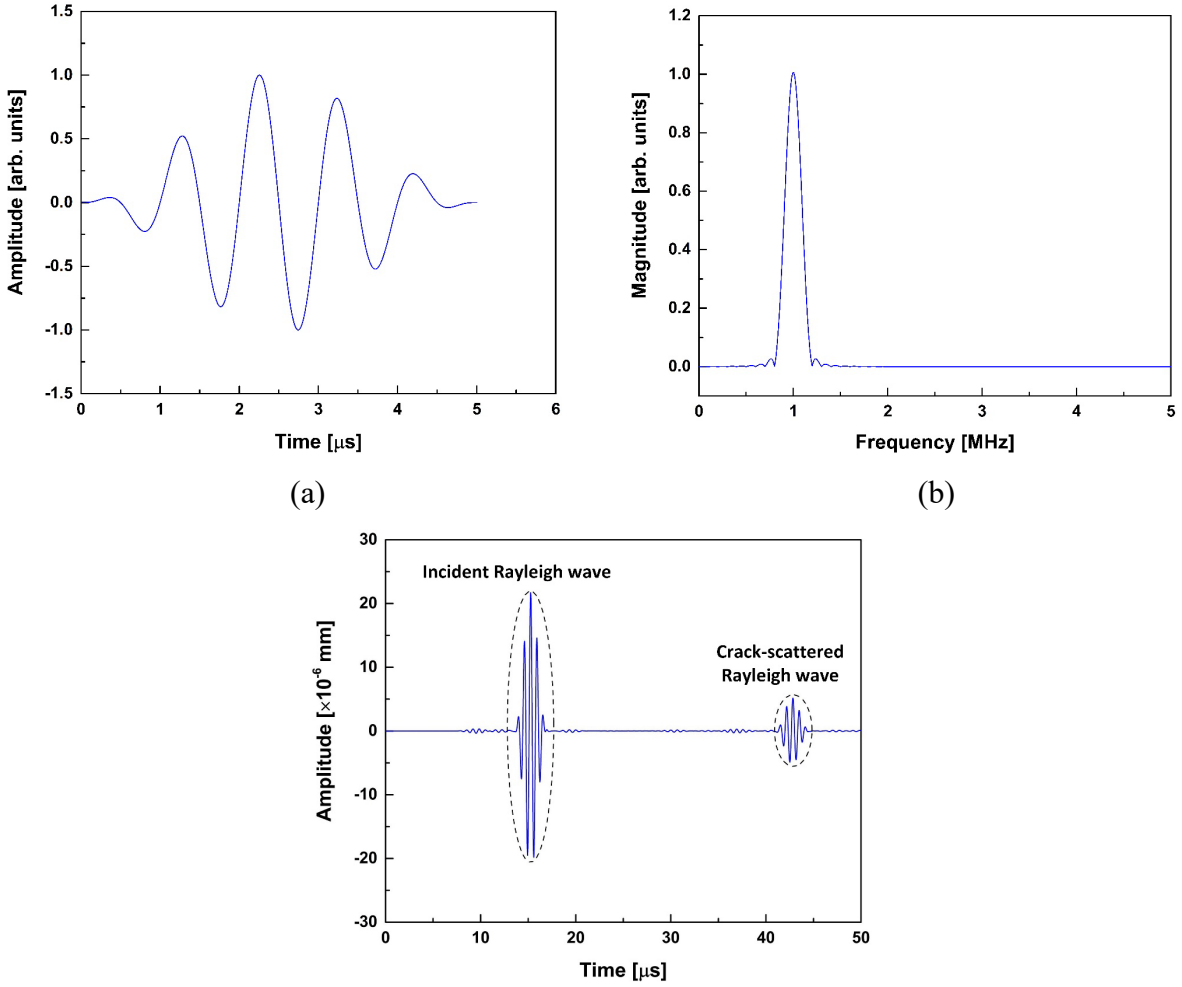

Figure 7. (a) A typical narrowband excitation signal with a central frequency of 1 MHz, (b) spectrum of the excitation signal, and (c) representative crack-scattered Rayleigh wave captured by a sensing point under the narrowband scenario.

To validate the frequency-dependent scattering of wideband laser-generated Rayleigh wave by a vertical surface crack, FE simulation is performed using a commercial software COMSOL Multiphysics® 6.0, to explore the interaction of laser-generated Rayleigh wave with a surface crack and obtain the resultant crack-scattered Rayleigh wavefield. The solid mechanics module, heat transfer module and the thermal expansion coupling module of the software are adopted to

simulate the generation of Rayleigh wave by a pulsed laser within the thermoelastic regime (in contrast to ablation regime, which can cause damage to the waveguide). The governing equation of the coupled temperature and displacement fields can be expressed as

$$\nabla^2 T - \frac{1}{\kappa}\dot{T} - \frac{1}{c^2}\ddot{T} = -\frac{q}{k}, \tag{7}$$

$$\mu\nabla^2 u + (\lambda+\mu)\nabla(\nabla\cdot u) = \rho\ddot{u} + \zeta\nabla T. \tag{8}$$

In the above, T and u are the temperature and displacement fields, respectively. κ is the thermal diffusivity, c the heat propagation velocity which is taken to be equal to the velocity of the longitudinal wave, and k the thermal conductivity. λ and μ are the Lame constants, ρ is the density and ζ represents the thermoelastic coupling coefficient: $\zeta = (3\lambda + 2\mu)\alpha_T$, where α_T is the linear thermal expansion coefficient. q is the heat source induced by the pulsed laser illumination.

The schematic of the FE model is shown in **Fig.8**. The length and depth of the model are 40 mm and 10 mm, respectively. The surface crack is located in the center of the top surface of the waveguide. The pulse duration and the radius of the laser beam is 12 ns and 0.1 mm, respectively. It is assumed that the heat flux within the laser beam has a Gaussian distribution, and the magnitude of the power intensity is 1.25×10^3 MW/m^2. To warranty the calculation accuracy of the heat flow in the vicinity of the pulsed laser, a very fine FE mesh in which the maximum grid size is 0.01 mm is adopted. For the outside of the vicinity of the laser beam where the heat flow attenuates greatly and the laser-generated ultrasonic waves dominate, the triangle mesh with a maximum size of 0.1 mm is used. Surface cracks with the depths varying from 0.2 mm to 0.6 mm are modeled, to investigate the scattering of wideband laser-generated Rayleigh wave by surface cracks with different severities. Two sensing points, locating at left and right side of the surface crack, are set to capture the back-scattered and transmitted waves, respectively.

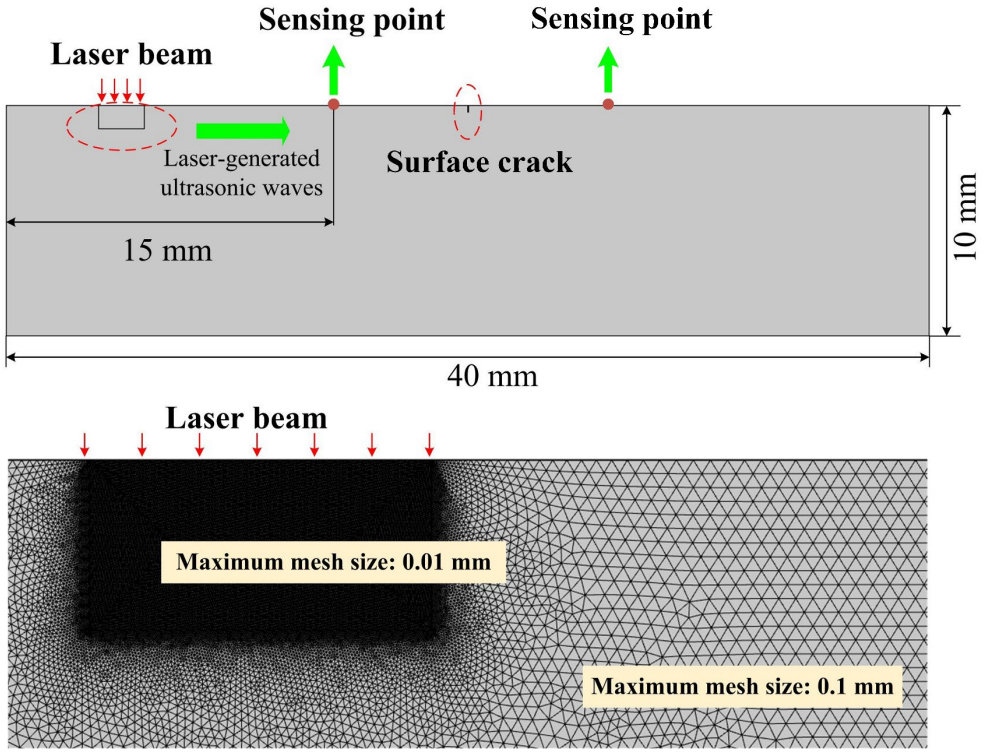

Figure 8. The schematic of the FE model for the simulation of laser-generated Rayleigh wave and the FE meshes around the laser beam.

3.2 Simulation Results and Discussions

For characterizing the scattering effect of a surface crack on a propagating narrowband Rayleigh wave, the dimensionless parameter β is calculated according to Eq. (5), based on the magnitudes of the crack-scattered and incident Rayleigh waves, as shown in **Fig. 7(c)**. Results of β of surface cracks with various depths versus the central frequency of the incident narrowband Rayleigh wave are depicted in **Fig. 9(a)**, from which it can be observed that the results of surface cracks with different depths share the same trend: β increases against the central frequency of the incident Rayleigh wave, reaches its maximum and then decreases, which agrees well with the theoretical results shown in **Fig. 2**.

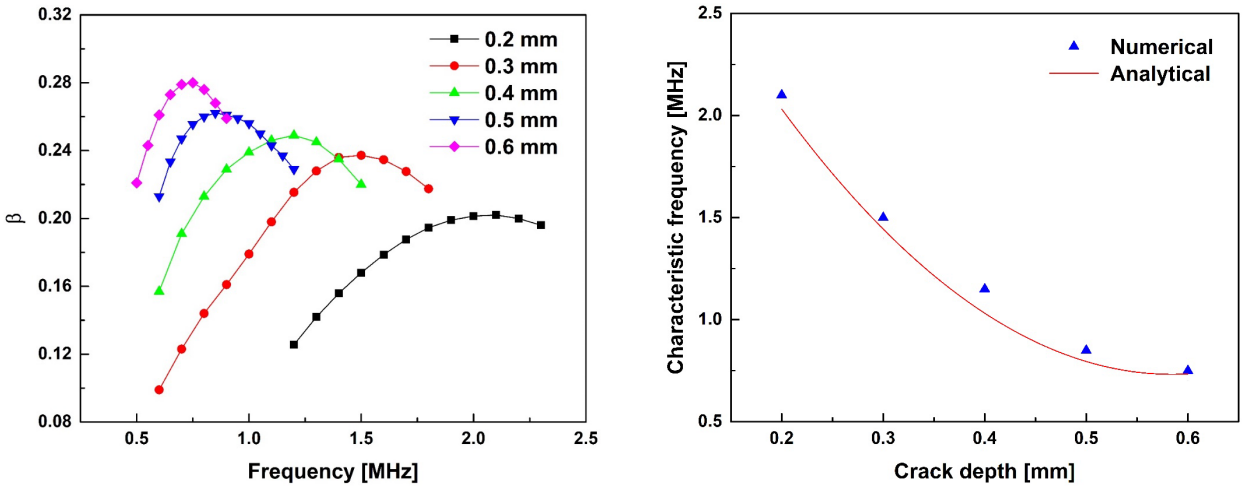

(a) (b)

Figure 9. (a) The dimensionless parameter of surface cracks with different depths with respect to the central frequency of the incident narrowband Rayleigh wave, and (b) the numerical results of characteristic frequency extracted from narrowband scenario as well as the comparison with the analytical results.

The characteristic frequency of each crack at which β reaches its maximum is extracted and compared with the analytical results (**Fig. 3**), as illustrated in **Fig. 9(b)**. Good agreement between the analytical and numerical results of the characteristic frequency of surface cracks verify the accuracy of the analytical modeling for the Rayleigh wave scattering in narrowband scenario in Section 2.1, which serves as the foundation for the investigation on the scattering of wideband laser-generated Rayleigh wave by a surface crack.

The wideband Rayleigh wave, as well as other types of ultrasonic waves, is generated by the pulsed laser beam in the multi-physical simulation. **Fig. 10** shows the displacement fields of the waveguide at different time (*i.e.*, 1.0 μs, 2.0 μs, 4.0 μs and 7.3 μs after the laser illumination). It can be observed that four kinds of ultrasonic waves are generated by the pulsed laser beam, including the Rayleigh wave (R), shear wave (S), body longitudinal wave (L), and skimming longitudinal wave (SL). As identified in **Fig. 10(d)**, after traversing the surface crack, the laser-generated Rayleigh wave is scattered by the crack, as a result of which the transmitted Rayleigh wave (TR) and the reflected Rayleigh wave (RR) propagates along and against the propagation direction of the incident laser-generated Rayleigh wave.

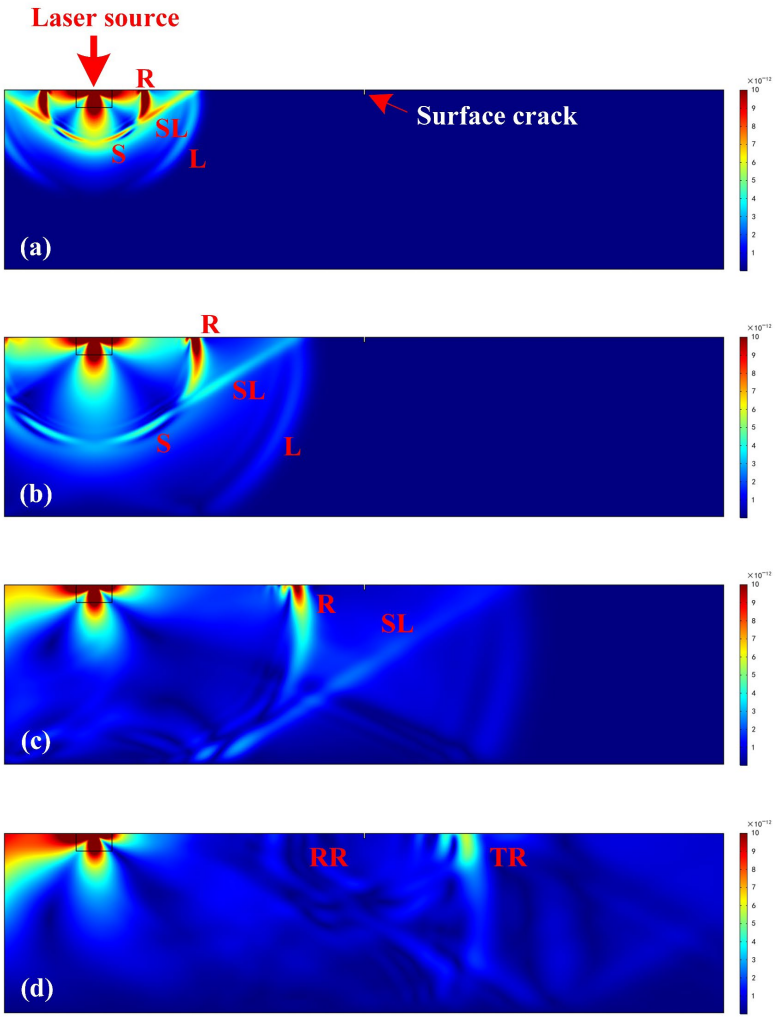

Figure 10. The displacement fields in the waveguide at (a) 1.0 μs, (b) 2.0 μs, (c) 4.0 μs, and 7.3 μs.

The displacement signals of the incident laser-generated Rayleigh wave and the back-scattered Rayleigh wave are captured by the sensing point at the left side of the surface crack. **Fig. 11** depicts the wave signals acquired from the waveguides that contain surface cracks with different depths (0.2 mm, 0.3 mm, 0.4 mm, 0.5 mm and 0.6 mm). It can be seen from the wave signals that the magnitude of the Rayleigh wave is remarkably larger than those of other types of waves, indicating that the Rayleigh wave dominates the laser-generated ultrasonic wavefields and the reflection and diffraction of other wave modes have weak influence on the scattered Rayleigh wave.

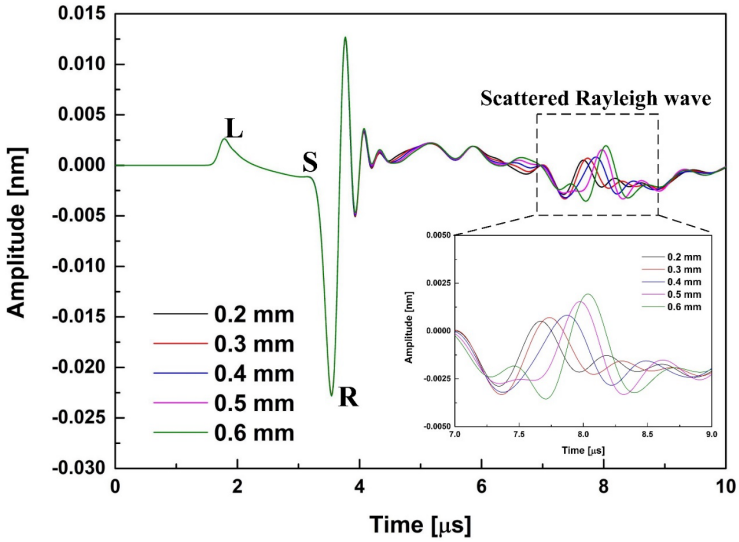

Figure 11. The incident laser-generated Rayleigh wave and its scattering by surface cracks with different depths.

The incident laser-generated Rayleigh wave and the back-scattered Rayleigh wave are extracted, respectively, and the fast Fourier transform is applied to obtain the spectra of the two waves. **Fig. 12** shows the spectra of the incident Rayleigh wave and the Rayleigh wave backscattered by surface cracks with different depths. It can be found that under different crack depth scenarios, the spectrum of the incident laser-generated Rayleigh wave is the same: the laser-generated Rayleigh wave has a central frequency of around 1.4 MHz and a broad frequency range of 0.5 ~ 3.5 MHz.

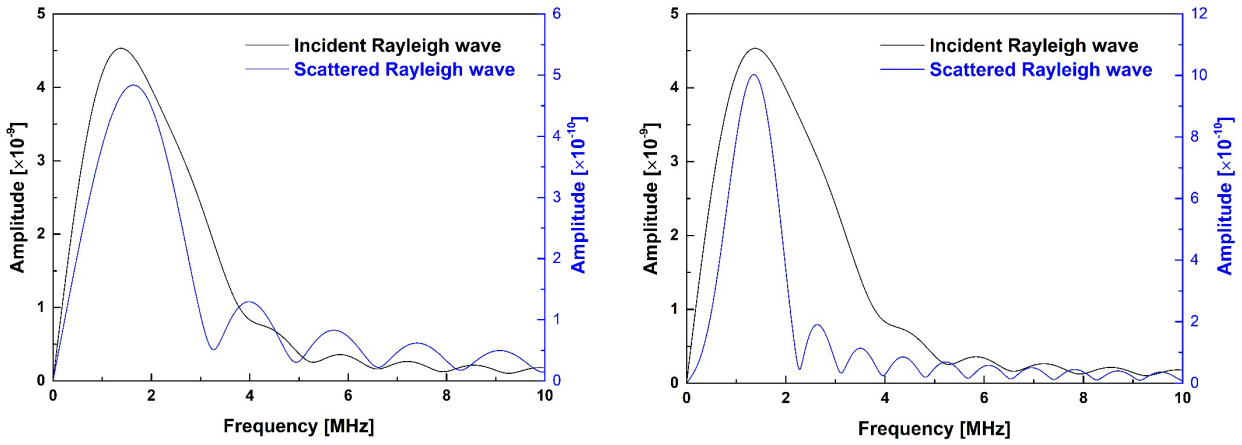

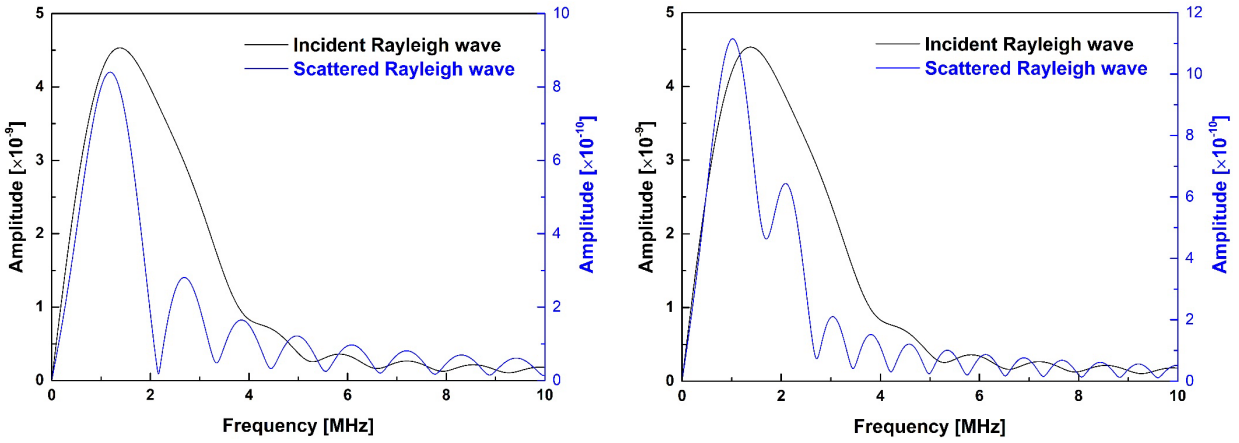

(c) (d)

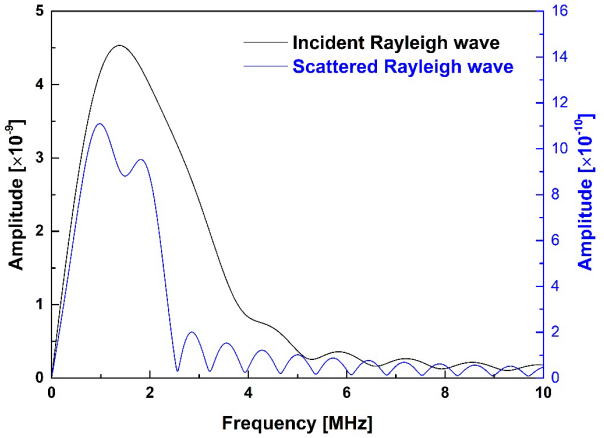

(e)

Figure 12. The spectra of the incident laser-generated Rayleigh wave and crack-scattered Rayleigh wave under the scenarios that the crack depth is (a) 0.2 mm, (b) 0.3 mm, (c) 0.4 mm, (d) 0.5 mm, (e) 0.6 mm.

The spectra of the Rayleigh wave backscattered by surface cracks with various depths are largely different from each other, revealing different scattering effect of surface cracks with various depths on a propagating Rayleigh wave. It can be observed that the central frequency of the scattered Rayleigh wave decreases with respect to the depth of the surface crack. According to Eq. (6), the SDI of different surface cracks can be calculated by comparing the spectra of incident and back-scattered Rayleigh waves, as shown in **Fig. 13(a)**. It can be found that for surface cracks with different depths, the SDI increases with respect to the frequency, reaches its maximum at the characteristic frequency and then decrease, which is in accordance with the analytical modeling in Section 2. The characteristic frequency of each surface crack is extracted and compared with the analytical results, as depicted in **Fig. 13(b)**, to observe good agreement between the two results,

which not only verify the accuracy of the analytical modeling of the scattering of Rayleigh wave by a surface crack, also demonstrate the effectiveness of the defined SDI and the characteristic frequency for quantitatively evaluating surface cracks using the wideband laser-generated Rayleigh wave.

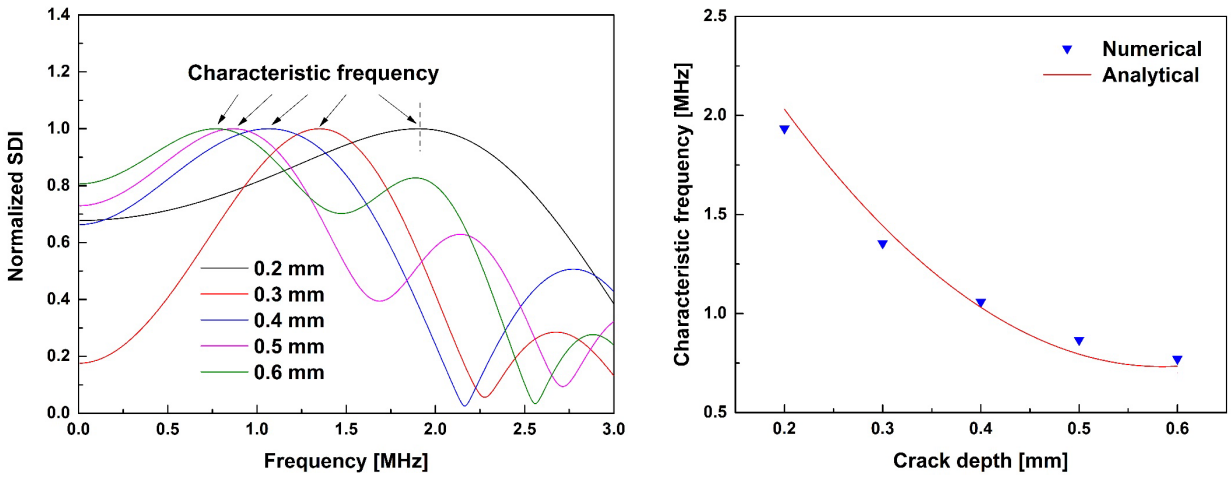

(a) (b)

Figure 13. (a) Normalized SDI of surface cracks with various depths determined by the back-scattered Rayleigh wave, and (b) the numerical results of characteristic frequency extracted from SDI as well as the comparison with the analytical results.

The SDI of different surface cracks determined by the spectra of incident and transmitted Rayleigh waves is depicted in **Fig. 14(a)**. It can be found that the SDI determined by transmitted wave decreases first with respect to the frequency, reaches its minimum at the characteristic frequency and then increases, which is also in accordance with the conclusion of the analytical modeling in Section 2. Based on the SDI determined by the transmitted Rayleigh wave, the characteristic frequency of each surface crack can be extracted and compared with the analytical results, as shown in **Fig. 14(b)**. Good agreement between the extracted characteristic frequency and the analytical results demonstrates that the transmitted Rayleigh wave can also be used to determine the characteristic frequency and subsequent surface crack evaluation.

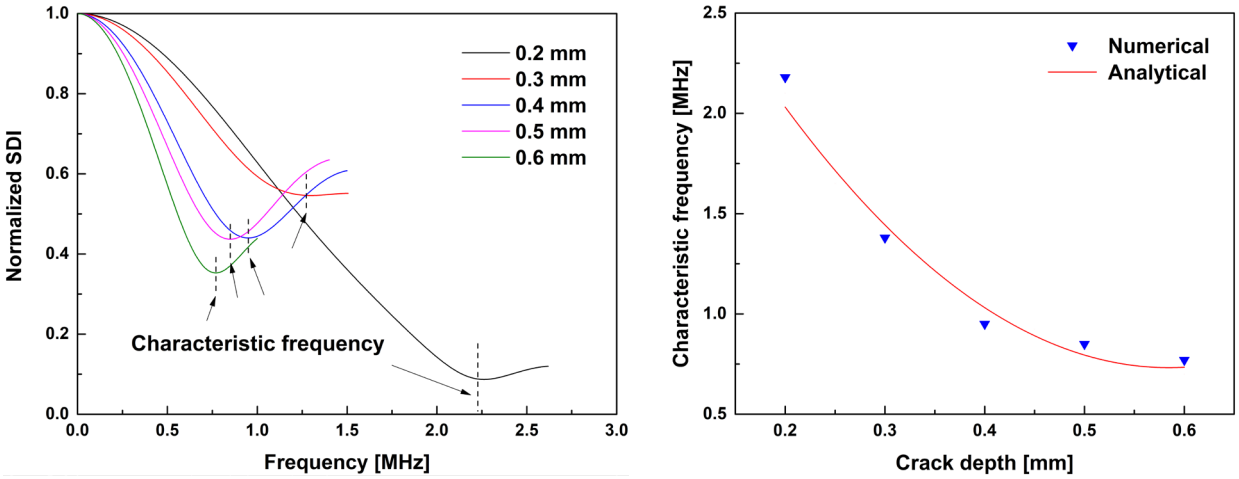

(a) (b)

Figure 14. (a) Normalized SDI of surface cracks with various depths determined by the transmitted Rayleigh wave, and (b) the numerical results of characteristic frequency extracted from SDI as well as the comparison with the analytical results.

In summary, FE simulation is performed to validate the frequency-dependent scattering of Rayleigh wave by a surface crack under both narrowband and wideband scenarios. For the narrowband scenario, the dimensionless parameter β is calculated based on the magnitudes of the incident and crack-scattered Rayleigh waves, via which the characteristic frequency can be determined. The numerical result of the characteristic frequency of a surface crack under the narrowband scenario is compared with the analytical results, and good agreement is achieved. For the wideband laser-generated Rayleigh wave, the SDI of surface cracks with various depths are calculated based on the spectra of the incident and crack-scattered (*i.e.*, back-scattered wave and transmitted wave) Rayleigh waves, and the characteristic frequency can be extracted by finding the extremum of the SDI. The numerical results of the characteristic frequency of a surface crack under the wideband scenario also agrees well with the analytical results, which demonstrate the potential of the frequency-scattering of laser-generated Rayleigh wave for surface crack evaluation.

4. Experimental Validation

Subsequent to FE validation, the effectiveness of the frequency-dependent scattering of a wideband Rayleigh wave for vertical surface crack characterization is verified experimentally. In the experiment, the wideband Rayleigh wave is generated by a pulsed laser, and vertical surface cracks in aluminum plates are evaluated by the frequency-dependent scattering effect of the surface crack on laser-generated Rayleigh wave.

4.1 Specimen and Test Set-up

Two plate-like aluminum specimens (measuring 300 mm long, 100 mm wide and 10 mm thick) are prepared, in each of which an artificial surface crack is fabricated using the high-speed electric discharge machine (EDM), as shown in **Fig. 15(a)**. The depths of the surface cracks in the two specimens are 0.4 mm and 0.6 mm, respectively. A compact Nd: YAG pulsed laser (QUANTEL® Centurion+ 50 mJ) with the operating wavelength of 1,064 nm and pulse duration of 12 ns is used to generate ultrasonic waves in the specimens. The pulsed laser is focused with optical lens towards a line source, as shown in **Fig. 15(b)**.

To avoid mounting two lead zirconate titanate (PZT) wafers in the short distance between the laser beam and the crack, which would result in strong disturbance on the original laser-generated Rayleigh wave, the PZT wafers are mounted at two sensing points (labeled as SP1 and SP2, respectively) which locate at different sides of the surface crack, to capture the incident and transmitted laser-generated Rayleigh wave. The ultrasonic waves are generated by the pulsed laser at four representative locations (labeled as L1, L2, L3 and L4), via which various combinations of the incident and transmitted laser-generated Rayleigh waves captured at SP1 and SP2 can be achieved, as summarized in Table 1.

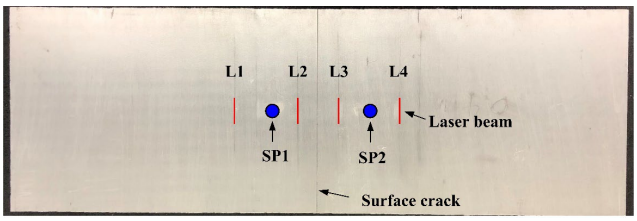

(a)

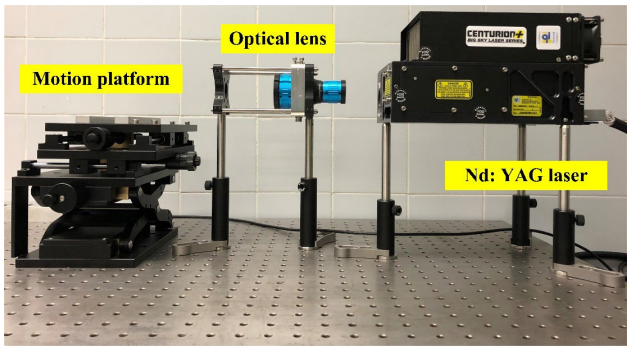

(b)

Figure 15. (a) Specimen used in the experiment, and (b) set-up of the experiment.

Table 1 Different combinations of incident and transmitted laser-generated Rayleigh waves captured at SP1 and SP2.

Excitation location	Incident laser-generated Rayleigh wave captured by	Transmitted Rayleigh wave captured by
L1	SP1	SP2
L2	SP1	SP2
L3	SP2	SP1
L4	SP2	SP1

4.2 Experimental Results

By way of illustration using the wave signals captured at SP1 and SP2 when the pulsed laser is located at L1, **Fig. 16(a)** depicts the time-domain signals of the incident laser-generated Rayleigh wave and the transmitted Rayleigh wave after passing the surface crack with the depth of 0.4 mm. It can be observed that the Rayleigh surface wave is generated by the pulsed laser and the Rayleigh wave dominates the wavefield of the laser-generated ultrasonic wave. The original wave signals are truncated quasi-empirically to extract the incident and transmitted Rayleigh waves. By performing frequency analysis with FFT, the spectra of the incident and transmitted Rayleigh

waves in frequency domain are obtained, as shown in **Fig. 16(b)**. According to the spectrum of the incident wave, the central frequency of the undistorted laser-generated Rayleigh wave is found to be around 1 MHz, and the Rayleigh wave is wideband with the wave energy mainly concentrated in the range of 0.5 ~ 2 MHz. It can be observed from the spectrum of the transmitted Rayleigh wave that the wave energy at 1 MHz decreases largely, owing to the scattering effect of the surface crack on the incident Rayleigh wave.

To characterize the vertical surface crack using the frequency-dependent scattering of laser-generated Rayleigh wave, the SDI is calculated as the ratio of the spectrum of the transmitted Rayleigh wave to that of the incident Rayleigh wave and illustrated in **Fig. 16(c)**. It can be found that the SDI reaches its minimum value at 0.952 MHz, revealing that the scattering effect of the surface crack on incident Rayleigh wave is the strongest at this frequency, which is defined as the characteristic frequency of a surface crack in analytical modeling of this study.

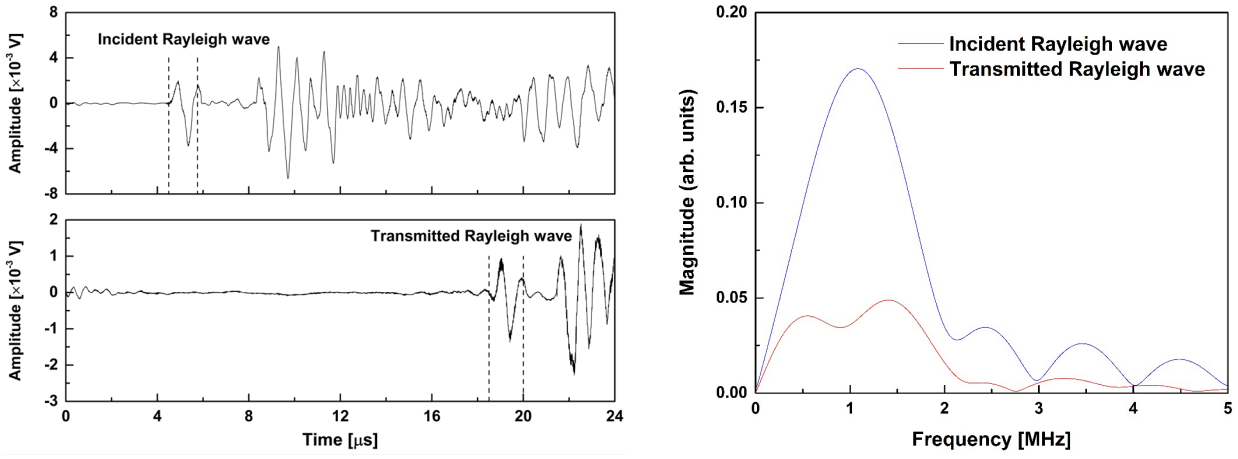

(a) (b)

Figure 16. (a) Time-domain signals and (b) frequency-domain spectra of the captured incident laser-generated Rayleigh wave and transmitted Rayleigh wave, and (c) transmission ratio calculated based on the frequency-domain spectra.

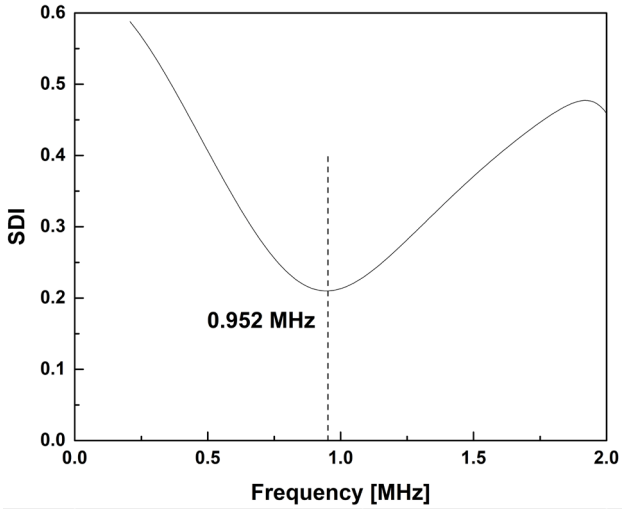

(c)

Figure 16. *Cont.*

Table 2 Experimental results of the characteristic frequencies of the surface cracks with the depths of 0.4 mm and 0.6 mm.

Crack depth (mm)	Characteristic frequency when excitation location at				Mean (MHz)	Relative error (%)
	L1	L2	L3	L4		
0.4	0.952	0.986	0.913	1.086	0.984	10.42
0.6	0.643	0.626	0.680	0.676	0.656	6.29

The characteristic frequencies of the surface crack (0.4 mm in depth) calculated based on the captured wave signals when the pulsed laser is located at L2, L3 and L4, as well as the experimental results of the surface crack with the depth of 0.6 mm, are summarized in Table 2. It can be seen from Table 2 that the experimental results of the characteristic frequencies of the two surface cracks agree with the theoretical results, not only verifying the model, also demonstrating the effectiveness of the frequency-dependent scattering of laser-generated wideband Rayleigh wave in characterizing surface cracks.

5. Concluding Remarks

In this study, the frequency-dependent Rayleigh wave scattering phenomenon in both narrowband and wideband scenarios is found based on the analytical solution to the magnitude of the Rayleigh

wave scattered by a surface crack. Starting from the explicit expression of the magnitude of crack-scattered narrowband Rayleigh wave, a dimensionless parameter β is defined as the ratio of the magnitude of the crack-scattered Rayleigh wave to that of the incident Rayleigh wave, to characterize the scattering effect of the surface crack on a propagating Rayleigh wave. By plotting β versus the frequency of the incident Rayleigh wave, it is observed that there exists a characteristic frequency for a surface crack, at which the scattering effect is the strongest. The frequency-dependent scattering of Rayleigh wave by a surface crack is further investigated in the wideband scenario (*i.e.*, laser-generated Rayleigh wave), in which the incident and the crack-scattered Rayleigh waves both have broad frequency ranges. An SDI is defined as the ratio of the spectrum of the crack-scattered Rayleigh wave to that of the incident Rayleigh wave, to characterize the scattering effect of a surface crack in the broad frequency range. It is found that the SDI of a surface crack also reaches its extremum at the characteristic frequency obtained from the narrowband scenario. FE simulation is performed to validate the frequency-dependent scattering of the Rayleigh wave by a vertical surface crack. The numerical results of the characteristic frequency in both scenarios quantitatively agree well with the analytical results. Experimental results demonstrate the effectiveness of the frequency-dependent scattering of the wideband laser-generated Rayleigh wave for vertical surface crack characterization.

Note that the surface crack examined in this study is different from a real three-dimensional (3D) surface crack which is defined with length and depth. The displacement field around a 3D crack decreases to zero at the endpoints of the crack in both length direction, making the explicit expression of the magnitude of the crack-scattered Rayleigh wave (Eqs. (3) and (4)) not tenable. Therefore, the characteristic frequency of a 3D crack deviates from the theoretical results derived based on the 2D model presented in this study. The extension of the 2D model to the 3D scenario needs further investigation.

Acknowledgement

L Xu acknowledges the support from CRD project of Hong Kong Productivity Council (No. 10013288). Z Su acknowledges the support from the Hong Kong Research Grants Council via General Research Funds (Nos. 15202820 and 15204419). The work was also supported by a General Project (No. 51875492) received from the National Natural Science Foundation of China.

References

[1] Xu L, Wang K, Su Y, He Y, Yang J, Yuan S, et al. Surface/sub-surface crack-scattered nonlinear rayleigh waves: A full analytical solution based on elastodynamic reciprocity theorem. Ultrasonics. 2022;118:106578.

[2] Xu L, Su Y, Wang K, Yang X, Yuan S, Su Z. An elastodynamic reciprocity theorem-based closed-form solution to second harmonic generation of lamb waves by a fatigue crack: Theory & experimental validation. Journal of Sound and Vibration. 2021;509:116226.

[3] Sun X, Liu H, Zhao Y, Qu J, Deng M, Hu N. The zero-frequency component of bulk waves in solids with randomly distributed micro-cracks. Ultrasonics. 2020;107:106172.

[4] Xu H, Cheng L, Su Z, Guyader J-L. Identification of structural damage based on locally perturbed dynamic equilibrium with an application to beam component. Journal of Sound and Vibration. 2011;330:5963-81.

[5] Shao W, Sun H, Wang Y, Qing X. A multi-level damage classification technique of aircraft plate structures using Lamb wave-based deep transfer learning network. Smart Materials and Structures. 2022;31:075019.

[6] Tong T, Hua J, Gao F, Zhang H, Lin J. Disbond contour estimation in aluminum/CFRP adhesive joint based on the phase velocity variation of Lamb waves. Smart Materials and Structures. 2022;31:095020.

[7] Jiang C, Zhang C, Li W, Deng M, Ng C-T. Assessment of damage in composites using static component generation of ultrasonic guided waves. Smart Materials and Structures. 2022;31:045025.

[8] Zhang Z, Liu M, Su Z, Xiao Y. Quantitative evaluation of residual torque of a loose bolt based on wave energy dissipation and vibro-acoustic modulation: A comparative study. Journal of Sound and Vibration. 2016;383:156-70.

[9] Wang X, Foliente G, Su Z, Ye L. Multilevel decision fusion in a distributed active sensor network for structural damage detection. Structural Health Monitoring. 2006;5:45-58.

[10] Li F, Meng G, Kageyama K, Su Z, Ye L. Optimal mother wavelet selection for lamb wave analyses. Journal of Intelligent Material Systems and Structures. 2009;20:1147-61.

[11] Su Z, Ye L. An intelligent signal processing and pattern recognition technique for defect identification using an active sensor network. Smart Materials and Structures. 2004;13:957.

[12] Wang K, Liu M, Su Z, Yuan S, Fan Z. Analytical insight into “breathing” crack-induced acoustic nonlinearity with an application to quantitative evaluation of contact cracks. Ultrasonics. 2018;88:157-67.

[13] Hong M, Mao Z, Todd MD, Su Z. Uncertainty quantification for acoustic nonlinearity parameter in Lamb wave-based prediction of barely visible impact damage in composites. Mechanical Systems and Signal Processing. 2017;82:448-60.

[14] Vanniamparambil P, Guclu U, Kontsos A. Identification of crack initiation in aluminum alloys using acoustic emission. Experimental Mechanics. 2015;55:837-50.

[15] Aggelis DG, Shiotani T, Polyzos D. Characterization of surface crack depth and repair evaluation using Rayleigh waves. Cement and Concrete Composites. 2009;31:77-83.

[16] Hy A, Ll A, Pqa B. Localization and size quantification of surface crack of concrete based on Rayleigh wave attenuation model - ScienceDirect. Construction and Building Materials.280.

[17] Aggelis DG, Shiotani T. Repair evaluation of concrete cracks using surface and through-transmission wave measurements. Cement & Concrete Composites. 2007;29:700-11.

[18] Jian X, Dixon S, Guo N, Edwards R. Rayleigh wave interaction with surface-breaking cracks. Journal of Applied Physics. 2007;101:064907.

[19] Ahmad M, Liu Z, Basit A, Wu B, He C. Characterization of surface crack width in plates using Rayleigh wave electromagnetic acoustic transducers. IOP Conference Series: Materials Science and Engineering. 2021;1043:042038 (14pp).

[20] Ching-Tai, Ng, Hasan, Mohseni, Heung-Fai, Lam. Debonding detection in CFRP-retrofitted reinforced concrete structures using nonlinear Rayleigh wave - ScienceDirect. Mechanical Systems and Signal Processing. 2019;125:245-56.
[21] Herrmann J, Kim JY, Jacobs LJ, Qu J, Littles JW, Savage MF. Assessment of material damage in a nickel-base superalloy using nonlinear Rayleigh surface waves. Journal of Applied Physics. 2006;99:1479-88.
[22] Kim G, In CW, Kim JY. Air-coupled detection of nonlinear Rayleigh surface waves in concrete-Application to microcracking detection. NDT & E International. 2014.
[23] Wang C, Kong Y, Wang W, Chen Z, Chen J, Zhu W, et al. Finite element analysis of laser-generated Rayleigh wave for sizing subsurface crack in frequency domain. Optik. 2022;260:169145.
[24] Tian Z, Howden S, Ma Z, Xiao W, Yu L. Pulsed laser-scanning laser Doppler vibrometer (PL-SLDV) phased arrays for damage detection in aluminum plates. Mechanical Systems and Signal Processing. 2019;121:158-70.
[25] Gao T, Sun H, Hong Y, Qing X. Hidden corrosion detection using laser ultrasonic guided waves with multi-frequency local wavenumber estimation. Ultrasonics. 2020;108:106182.
[26] Cavuto A, Martarelli M, Pandarese G, Revel G, Tomasini E. Train wheel diagnostics by laser ultrasonics. Measurement. 2016;80:99-107.
[27] Shi W, Tong Y, Lu C, Chen Y, Shen G, Zeng G. Improving laser-EMAT ultrasonic energy conversion efficiency using surface constraint mechanism. Ultrasonics. 2022;124:106729.
[28] Xiao J, Chen J, Yu X, Lisevych D, Fan Z. Remote characterization of surface slots by enhanced laser-generated ultrasonic Rayleigh waves. Ultrasonics. 2022;119:106595.
[29] Jian X, Fan Y, Edwards R, Dixon S. Surface-breaking crack gauging with the use of laser-generated Rayleigh waves. Journal of Applied Physics. 2006;100:064907.
[30] Liu P, Jang J, Yang S, Sohn H. Fatigue crack detection using dual laser induced nonlinear ultrasonic modulation. Optics and Lasers in Engineering. 2018;110:420-30.
[31] Zhou Z, Zhang K, Zhou J, Sun G, Wang J. Application of laser ultrasonic technique for non-contact detection of structural surface-breaking cracks. Optics & Laser Technology. 2015;73:173-8.
[32] Chen D, Lv G, Guo S, Zuo R, Liu Y, Zhang K, et al. Subsurface defect detection using phase evolution of line laser-generated Rayleigh waves. Optics & Laser Technology. 2020;131:106410.
[33] Zeng W, Qi S, Liu L, Yao Y. Research on laser-generated Rayleigh waves with angled surface crack by finite element method. Optik. 2019;181:57-62.
[34] Zeng W, Yao Y, Qi S, Liu L. Finite element simulation of laser-generated surface acoustic wave for identification of subsurface defects. Optik. 2020;207:163812.
[35] Zeng W. Numerical simulation of laser-generated ultrasonic waves for identification of branched-breaking defects. Optik. 2020;208:164435.
[36] Zeng W, Yao Y. Numerical simulation of laser-generated ultrasonic waves for detection surface defect on a cylinder pipe. Optik. 2020;212:164650.
[37] Xu L, Wang K, Yang X, Su Y, Yang J, Liao Y, et al. Model-driven fatigue crack characterization and growth prediction: a two-step, 3-D fatigue damage modeling framework for structural health monitoring. International Journal of Mechanical Sciences. 2021;195:106226.
[38] Phan H, Cho Y, Achenbach JD. Application of the reciprocity theorem to scattering of surface waves by a cavity. International Journal of Solids and Structures. 2013;50:4080-8.
[39] Lee J, Achenbach JD, Cho Y. Use of the reciprocity theorem for a closed form solution of scattering of the lowest axially symmetric torsional wave mode by a defect in a pipe. Ultrasonics. 2018;84:45-52.
[40] Dubuc B, Livadiotis S, Ebrahimkhanlou A, Salamone S. Crack-induced guided wave motion and modal excitability in plates using elastodynamic reciprocity. Journal of Sound and Vibration. 2020;476:115287.

[41] Kubrusly AC, Dixon S. Application of the reciprocity principle to evaluation of mode-converted scattered shear horizontal (SH) wavefields in tapered thinning plates. Ultrasonics. 2021;117:106544.
[42] Achenbach J, Achenbach J. Reciprocity in elastodynamics: Cambridge University Press; 2003.
[43] Balogun O, Achenbach JD. Application of the reciprocity theorem to scattering of surface waves by an inclined subsurface crack. International Journal of Solids and Structures. 2020;207:82-8.